Preparation of Silver-Palladium Alloyed Nanoparticles for Plasmonic Catalysis under Visible-Light Illumination

Peiris, Erandi

2020-08

Peiris , E , Hanauer , S , Knapas , K & Camargo , P H C 2020 , ' Preparation of Silver-Palladium Alloyed Nanoparticles for Plasmonic Catalysis under Visible-Light Illumination ' , Journal of Visualized Experiments , no. 162 , 61712 . https://doi.org/10.3791/61712

http://hdl.handle.net/10138/346535
https://doi.org/10.3791/61712

acceptedVersion

TITLE:

Preparation of silver-palladium alloyed nanoparticles for plasmonic catalysis under visible-light illumination

AUTHORS AND AFFILIATIONS:

Erandi Peiris, Sébastien Hanauer, Kjell Knapas, and Pedro H. C. Camargo*

Department of Chemistry, University of Helsinki, A.I. Virtasen aukio 1, Helsinki, Finland

Corresponding author:
Pedro H. C. Camargo (pedro.camargo@helsinki.fi)

Email addresses of co-authors:
Erandi Peiris (erandi.prangige@helsinki.fi)
Sébastien Hanauer (sebastien.hanauer@helsinki.fi)
Kjell Knapas (kjell.knapas@helsinki.fi)

KEYWORDS:

Plasmonic catalysis, localized surface plasmon resonance, bimetallic nanoparticles, alloyed nanoparticles, silver, palladium, photocatalysis

SUMMARY:

Presented here is a protocol for the synthesis of silver-palladium (Ag-Pd) alloy nanoparticles (NPs) supported on ZrO_2 (Ag-Pd/ZrO_2). This system allows the harvesting of energy from visible light irradiation to accelerate and control molecular transformations. This is illustrated by performing the nitrobenzene reduction under light irradiation catalyzed by Ag-Pd/ZrO_2 NPs.

ABSTRACT:

It has been demonstrated that the localized surface plasmon resonance (LSPR) in plasmonic nanoparticles (NPs) can contribute to accelerate and control the selectivity of a variety of molecular transformations. This opens possibilities for the use of visible or near-IR light as a sustainable input to drive and control reactions when plasmonic nanoparticles support LSPR excitation in these ranges are employed as catalysts. Unfortunately, this is not the case for several catalytic metals such as palladium (Pd). One strategy to overcome this limitation is to employ bimetallic NPs containing plasmonic and catalytic metals. In this case, the LSPR excitation in the plasmonic metal can contribute to accelerate and control transformations driven by the catalytic component. The method reported herein focuses on the synthesis of bimetallic silver-palladium (Ag-Pd) NPs supported on ZrO_2 (Ag-Pd/ZrO_2) that acts as a plasmonic-catalytic system. The NPs were prepared by co-impregnation of corresponding metal precursors on the ZrO_2 support

followed by simultaneous reduction. This leads to the formation of bimetallic NPs directly on the ZrO_2 support. The Ag-Pd/ZrO_2 NPs were then used as plasmonic catalysts for the reduction of nitrobenzene under 425 nm illumination by LED lamps. Using gas chromatography (GC), the conversion and selectivity of the reduction reaction under the dark and light irradiation conditions can be monitored, demonstrating the enhanced catalytic performance and control over selectivity under LSPR excitation after alloying non-plasmonic Pd with plasmonic metal Ag. This technique can be adapted to a wide range of molecular transformations and NPs compositions, making it possible for the characterization of the plasmonic catalytic activity of different types of catalysis in terms of conversion and selectivity.

INTRODUCTION:

Among the several applications of metal nanoparticles (NPs), catalysis deserves special attention. Catalysis plays a central role in a sustainable future, contributing to less energy consumption, better utilization of raw materials, and enabling cleaner reaction conditions[1–4]. Thus, progress in catalysis can provide tools for enhancing the atomic efficiency of chemical processes, making them cleaner, more economic viable, and more environmentally-friendly. Metal NPs encompassing silver (Ag), gold (Au) or copper (Cu) can display interesting optical properties in the visible range that arise from the unique way these systems interact with light at the nanoscale *via* the localized surface plasmon resonance (LSPR) excitation[5–8]. In these NPs, referred to as plasmonic NPs, the LSPR comprises the resonant interaction between the incident photons (from an incoming electromagnetic wave) with the collective motion of electrons[5–8]. This phenomenon takes place at a characteristic frequency which is dependent on size, shape, composition, and dielectric constant of the environment, for example[9–11]. For Ag, Au, and Cu, these frequencies can range from the visible to the near-IR, opening up possibilities for the utilization of solar energy to excite their LSPR[5–8, 12, 13].

Recently, it has been demonstrated that the LSPR excitation in plasmonic NPs can contribute to accelerate the rates and control the selectivity of molecular transformations[5, 14–19]. This gave birth to a field called plasmonic catalysis, which focus on using energy from light to accelerate, drive, and/or control chemical transformations.[5, 14–19] In this context, it has been established that the LSPR excitation in plasmonic NPs can lead to the formation of energetic hot electrons and holes, referred to as LSPR-excited hot carriers. These carriers can interact with adsorbed species through electronic or vibrational activation[15, 16]. In addition to increased reaction rates, this process can also provide alternative reaction pathways not accessible via traditional thermochemically-driven processes, opening up new avenues for the control over reaction selectivity[20–25]. Importantly, it is worth noting that the plasmon decay can also lead to thermal dissipation, leading to a temperature increase in the vicinity of the NPs which can also contribute to speed up reaction rates[15, 16].

Due to these interesting features, plasmonic catalysis has been successfully employed towards a variety of molecular transformations[18]. Nevertheless, an important challenge remains. While plasmonic NPs such as Ag and Au display excellent optical properties in the visible and near-IR ranges, their catalytic properties are limited in terms of the scope of transformations. In other words, they do not display good catalytic properties for several of transformations. Additionally, metals that are important in catalysis, such as palladium (Pd) and platinum (Pt), do not support

LSPR excitation in the visible or near-IR ranges. To bridge this gap, bimetallic NPs containing a plasmonic and catalytic metal represents an effective strategy[20, 26–29]. In these systems, the plasmonic metal can be employed as an antenna to harvest energy from the light excitation through the LSPR, which is then used to drive, accelerate, and control molecular transformations at the catalytic metal. Thus, this strategy enables us to extend plasmonic catalysis beyond traditional plasmonic metal NPs[20, 26–29].

This protocol describes the facile synthesis of bimetallic silver-palladium (Ag-Pd) alloyed NPs supported on ZrO_2 (Ag-Pd/ZrO_2) that can act as a plasmonic-catalytic system for plasmonic catalysis. The Ag-Pd/ZrO_2 NPs were prepared by co-impregnation of the corresponding metal precursors on the ZrO_2 support followed by simultaneous reduction[30]. This approach led to the formation of bimetallic NPs around 10 nm in size (diameter) directly at the surface of the ZrO_2 support. The NPs were composed of 1 mol % of Pd to minimize the utilization of the catalytic metal while maximizing the optical properties of the resulting Ag-Pd NPs. A protocol for the application of the Ag-Pd/ZrO_2 NPs in plasmonic catalysis was demonstrated towards the reduction of nitrobenzene. We employed 425 nm LED illumination for the LSPR excitation. By using gas chromatography, it is described how to monitor the conversion and selectivity of the reduction reaction under the dark and light irradiation conditions. It is shown that the LSPR excitation led to enhanced catalytic performance and control over selectivity in Ag-Pd/ZrO_2 NPs relative to purely thermally driven conditions. The method described in this video protocol is based on a simple photocatalytic reaction setup coupled with gas chromatography, and can be adapted to a wide range of molecular transformations and NPs compositions. Thus, this method makes possible the characterization of photocatalytic activity, in terms of conversion and reaction selectivity, of different NPs and for a myriad of liquid-phase transformations. We believe the video protocol will give important guidelines and insights to both newcomers and more experienced scientists in the field.

PROTOCOL:

1. Synthesis of Ag-Pd/ZrO_2 NPs

NOTE: In this procedure, the Pd mol % in Ag-Pd corresponded to 1 %, and the Ag-Pd loading on ZrO_2 corresponded to 3 wt. %

1.1. Place 1 g of ZrO_2 powder in a 250 mL beaker.

1.2. Add 50 mL of an $AgNO_3$ (aq) (0.0059 mol/L) and 9.71 mL of a K_2PdCl_4 (aq) (0.00031 mol/L) solutions to the beaker under vigorous magnetic stirring (500 rpm) at room temperature.

1.3. Add 10 mL of lysine (0.53 M) aqueous solution.

1.4. Keep the mixture under vigorous stirring (500 rpm) for 20 min.

1.5. After 20 min, use a pipette to add to the suspension 10 mL of a freshly prepared $NaBH_4$ (aq) (0.035 M) solution dropwise, at a rate of 1 mL/min. Keep the suspension under stirring (500 rpm)

throughout the process.

1.6. Let the mixture stir for 30 min at room temperature.

2. Separation and purification of the catalyst

2.1. Transfer the suspension to centrifuge tubes and separate the solids from the mixture by centrifugation at 3260 x *g* for 10 min.

2.2. Carefully remove the liquid phase with a pipette and add 15 mL deionized water to the tubes.

2.2.1. Shake vigorously until the dispersion of the solid. If you cannot achieve good dispersion, place the tubes in an ultrasonic bath for 5 min.

2.2.2. Centrifuge the dispersion at 3260 x *g* for 10 min.

2.3. Repeat the washing steps (2.2. to 2.2.2.) two more times using deionized water, then once using ethanol instead of water.

2.4. Remove the ethanol and dry the solid in an oven at 60 °C for 24 h.

2.5. The prepared Ag-Pd/ZrO_2 NPs can then be characterized by a variety of microscopy, elemental, and spectroscopic techniques.

3. Synthesis of Ag/ZrO_2 NPs

NOTE: In this procedure Ag loading on ZrO_2 corresponded to 3 wt. %

3.1. Place 1 g of ZrO_2 powder in a 250 mL beaker.

3.2. Add 50 mL of an $AgNO_3$ (aq) (0.0059 mol/L) solution to the beaker under vigorous magnetic stirring (500 rpm) at room temperature.

3.3. Add 10 mL of lysine (0.53 M) aqueous solution.

3.4. Keep the mixture under vigorous stirring (500 rpm) for 20 min.

3.5. After 20 min, use a pipette to add to the suspension 10 mL of a freshly prepared $NaBH_4$ (aq) (0.035 M) solution dropwise, at a rate of 1 mL/min. Keep the suspension under stirring (500 rpm) throughout the process.

3.6. Let the mixture stir for 30 min under room temperature.

4. Separation and purification of the catalyst

4.1. Transfer the suspension to centrifuge tubes and separate the solids from the mixture by centrifugation at 3260 x *g* for 10 min.

4.2. Carefully remove the liquid phase with a pipette and add 15 mL deionized water to the tubes.

4.2.1. Shake vigorously until the dispersion of the solid. If you cannot achieve good dispersion, place the tubes in an ultrasonic bath for 5 min.

4.2.2. Centrifuge the dispersion at 3260 x *g* for 10 min.

4.3. Repeat the washing steps (4.2. to 4.2.2.) two more times using deionized water, then once using ethanol instead of water.

4.4. Remove the ethanol and dry the solid in an oven at 60 °C for 24 h.

4.5. The prepared Ag/ZrO_2 NPs can then be characterized by a variety of microscopy, elemental, and spectroscopic techniques.

5. Investigation of plasmonic catalytic performance towards the nitrobenzene reduction under LSPR excitation (light illumination)

5.1. Place 30 mg of catalyst in a 25 mL round-bottom flask along with a magnetic stirring bar.

5.2. Add to the reactor 5 mL of a solution of nitrobenzene (0.03 mol/L) in isopropyl alcohol (IPA).

5.3. Then, add 11.22 mg of KOH powder (0.0002 mol).

5.4. Purge the reactor by bubbling the suspension with an argon flow for 1 min. Immediately after purging, seal the flask.

5.5. Place the reactor in an oil bath heated at 70 °C above a temperature-controlled magnetic stirrer (500 rpm).

5.6. Irradiate the tube using 4 LED lamps with a wavelength of 425 nm as the light source, and a light intensity of 0.5 W/cm^2 as described in Figure 4. The distance from the lamps to the reaction flask should be 7 cm.

5.7. Let the reaction proceed for 2.5 h at 70 °C under vigorous magnetic stirring (500 rpm).

5.8. Then, turn the light off, open the reactor and use a syringe and a needle to collect a 1 mL sample. Filter it through a Millipore filter (pore size 0.45 µm), to remove the catalyst particulates, into a gas chromatography vial.

6. Reaction in the absence of LSPR excitation (dark conditions)

6.1. Follow the same steps as described in 5, but without light irradiation. Wrap the reaction tube with aluminium foil to prevent any light exposure.

7. Gas chromatography (GC) analysis preparation

7.1. Prepare an IPA solution containing approximately 30 mmol/L nitrobenzene (NB), 30 mmol/L of aniline (AN), and 30 mmol/L of azobenzene (AB).

7.2. Run a GC analysis of the solution using a suitable method. Different methods can be tested by varying the column temperature and gas flow programs. The selected method should be able to separate the peaks corresponding to IPA, NB, AN, and AB in the minimum period of retention time.

7.3. Once the method has been selected, prepare a set of solutions of 50 mM, 25 mM, 10 mM, 5 mM and 2.5 mM NB in IPA, and another set of solutions of AN and AB in IPA with the same concentrations.

7.4. Run a GC analysis of the prepared solutions. Each chromatogram should present 2 peaks: the higher one corresponds to IPA and the lower one corresponds to NB, AN, or AB. For each chromatogram, note down the retention time and peak area of all the peaks.

7.5. Trace the calibration curves of NB, AN, and AB by plotting the concentration versus peak area of each sample.

8. GC analysis

8.1. Run a GC analysis on the samples collected in steps 5. and 6. with the same method used for steps 7.2. and 7.4.

8.2. For each chromatogram, note down the retention time and peak area and use the calibration curves plotted previously to determine the concentration of NB, AN, and AB in the samples.

8.3. Calculate the nitrobenzene conversion as well as the aniline and azobenzene selectivity using the equations:

$$Conversion\ (\%) = \frac{C_{NB}^{0} - C_{NB}}{C_{NB}^{0}} * 100$$

$$AN\ Selectivity\ (\%) = \frac{C_{AN}}{C_{NB}^{0} - C_{NB}} * 100$$

$$AB\ Selectivity\ (\%) = \frac{C_{AB}}{C_{NB}^{0} - C_{NB}} * 100$$

Where C_{NB}^{0} is the initial NB concentration (0.03 mol/L), and C_{NB}, C_{AN}, C_{AB} correspond to the NB, AN, and AB concentrations, respectively, after 2.5 hours reaction by the GC analysis.

REPRESENTATIVE RESULTS:

Figure 1A shows digital photographs of the solid samples containing the pure ZrO_2 oxide (left) and the Ag-Pd/ZrO_2 NPs (right). This change in color from white (in ZrO_2) to brown (Ag-Pd/ZrO_2) provides the initial qualitative evidence on the deposition of Ag-Pd NPs at the ZrO_2 surface. Figure 1B shows the UV-visible absorption spectra from the Ag-Pd/ZrO_2 NPs (blue trace) as well as ZrO_2 (black trace) and Ag/ZrO_2 NPs (red trace). Here, the ZrO_2 support and Ag/ZrO_2 NPs were employed as reference materials. ZrO_2 did not display any bands in the visible range. Therefore, it should not contribute to any photocatalytic activity. A signal centered at 428 nm could be detected for the Ag/ZrO_2 NPs (red trace). This signal is assigned to the LSPR dipolar mode in Ag NPs[9]. The Ag-Pd/ZrO_2 NPs displayed a peak centered at 413 nm which is slightly blue-shifted and lower in intensity relative to the Ag/ZrO_2 NPs. The blue shift could be assigned to the change in material permittivity upon alloying with Pd[31]. Also, the decrease in the peak intensity is evidence on the formation of alloyed Ag-Pd NPs, as it is well established that the addition of a non-plasmonic metal to a plasmonic nanoparticle leading to core-shell or alloyed systems lead to the damping in the intensity of the LSPR peak[32]. It is important to note that in this case, we kept the Pd wt. % in the Ag-Pd NPs low (~1 %) so that the LSPR peak is not completely suppressed and the Ag-Pd samples still retain optical properties (LSPR excitation) in the visible range and therefore are active for plasmonic catalysis.

[Place **Figure 1** here]

During the synthesis of the catalysts, the amount of Ag and Pd salt used were calculated in order to reach 3 wt. % metal loading on the support, and a composition of 99 % Ag and 1 % Pd by weight (wt. %) for Ag-Pd/ZrO_2. To verify the composition of the catalysts, an Atomic Emission Spectroscopy (AES) study was conducted (MP-AES 4200 from Agilent Technologies). Calculated amounts of Ag/ZrO_2 and Ag-Pd/ZrO_2 were digested in concentrated nitric acid. The obtained solutions were then analyzed by AES and the amount of Ag initially present in the catalysts was deduced from calibration curves. To determine the Pd content of Ag-Pd/ZrO_2, the same process was employed, except that the catalyst was digested using *aqua regia*. The AES results revealed that the metal loading was 2.6 wt. % for both catalysts, while the composition of the Ag-Pd was 1 wt. % Pd as expected.

Figures 2A-C show scanning (SEM, Figure 2A) and transmission electron microscopy (TEM, Figure 2B) of the Ag-Pd/ZrO_2 NPs. The Ag-Pd NPs at the surface of the ZrO_2 supports are difficult to be identified from SEM images (Figure 2A) due to their small NPs sizes. However, the formation of Ag-Pd NPs with mean particle size around 10 nm (Figure 2C) in diameter can be identified from the TEM images (some of them are indicated by the arrows in Figure 2B for clarity). They displayed a spherical shape and a relatively uniform dispersion over the surface of the ZrO_2

supports.

[Place **Figure 2** here]

After the synthesis of Ag-Pd NPs supported on ZrO_2, this method focused on application as alloyed systems in plasmonic catalysis. Specifically, it describes the utilization of the reduction of nitrobenzene as a model transformation in the liquid phase as illustrated in Figure 3. This probe reaction is interesting as the reduction of nitrobenzene can lead to the formation of azobenzene and aniline[33, 34]. Therefore, this model transformation enables the simultaneous investigation of conversion percentages and reaction selectivity as a function of the light illumination (LSPR excitation) in plasmonic catalysis. Here, the reaction was performed in the presence of isopropanol as the solvent and KOH. Also, 70 ^{o}C was employed as the reaction temperature, four 425 nm LED lamps were employed as the light illumination source, and 2.5 h was the reaction time (as described in section 5. of the protocol). In addition to the use of Ag-Pd/ZrO_2 NPs as plasmonic catalysts, blank reactions (absence of catalyst), and Ag/ZrO_2 NPs as reference catalysts to demonstrate the role of Pd in the alloyed bimetallic NPs were also described.

[Place **Figure 3** here]

Figures 4A and B show a scheme (Figure 4A) and a digital photograph (Figure 4B) of the reactor and lamps setup employed in the plasmonic catalysis investigation. The setup used for LSPR excitation was made of four 425 nm LED lamps equally spaced around the reactor, at a distance of 7 cm. The reactor was positioned in the center of the system, immersed in an oil bath over a temperature-controlled magnetic stirrer. This enables control over the temperature and more uniform illumination of the reaction mixture from all directions.

[Place **Figure 4** here]

After the reaction proceeds, the conversion and selectivity for the formation of azobenzene and aniline can be measured by gas chromatography. Figures 5A and B show the chromatograms obtained at the end of the reaction catalyzed by Ag-Pd/ZrO_2 NPs that was carried out under LSPR excitation (Figure 5A) and dark conditions (Figure 5B). In this case, one must ensure to use a GC method that enables the separation of nitrobenzene, azobenzene, and aniline in different retention times to correctly identify these molecules, while calibration curves for each molecule were employed to perform their quantification. Moreover, the reaction mixture can also be analyzed by gas chromatography-mass spectrometry (GC-MS) to confirm the formation of azobenzene and aniline and also for any other products that could be formed.

[Place **Figure 5** here]

Table 1 and Figures 6A and B depict the conversion percentages for the nitrobenzene reduction (Figure 6A) and the selectivity towards azobenzene and aniline (Figure 6B) under light illumination for the alloyed Ag-Pd/ZrO_2 NPs as well as for Ag/ZrO_2 NPs. In the absence of any

catalysts (blank reactions), no nitrobenzene conversion was detected both in the presence and absence of light illumination. For Ag/ZrO_2 NPs, while no conversion was detected in the dark, a 36 % conversion was observed under LSPR excitation. A 56 % selectivity towards azobenzene (18 % selectivity towards aniline) was detected. This result indicates that the Ag alone can catalyze this reaction under LSPR excitation. For the bimetallic $Ag\text{-}Pd/ZrO_2$ NPs, no significant conversion was detected under dark conditions (2.2 %). Interestingly, under LSPR excitation, the conversion % corresponded to 63 %, with a 73 % selectivity towards azobenzene (27 % selectivity towards aniline). This observation demonstrates the potential of the bimetallic configuration in plasmonic-catalytic nanoparticles not only to increase conversion under LSPR excitation but also to control reaction selectivity.

[Place **Table 1** here]

[Place **Figure 6** here]

FIGURE AND TABLE LEGENDS:

Figure 1: Optical characterization of the catalysts. (A) digital photography of the solid ZrO_2 supports (left) and $Ag\text{-}Pd/ZrO_2$ catalyst (right). **(B)** UV-Visible extinction spectra of ZrO_2, Ag/ZrO_2, and $Ag\text{-}Pd/ZrO_2$ catalysts. The spectra were recorded using an integration sphere in Diffuse Reflectance Spectra (DRS) mode.

Figure 2: Morphological analysis of the $Ag\text{-}Pd/ZrO_2$ catalyst. (A) SEM image of the $Ag\text{-}Pd/ZrO_2$ catalyst. **(B)** TEM image of the $Ag\text{-}Pd/ZrO_2$ catalyst. The white arrows in depict examples of regions containing Ag-Pd NPs. **(C)** Histogram of the size distribution of Ag-Pd NPs on the $Ag\text{-}Pd/ZrO_2$ catalyst.

Figure 3: Schematic representation of the model reaction. Scheme of the photocatalyzed nitrobenzene reduction used as model reaction. Under LSPR excitation, this reaction leads to the formation of azobenzene and aniline as products.

Figure 4: Representation of the photocatalytic reaction set-up. (A) Top-view scheme and **(B)** digital photography of the light reaction setup including the reactor in an oil bath surrounded by four 425 nm LED lamps positioned at a distance of 7 cm away from the reactor.

Figure 5: Chromatograms of the reaction mixture. GC chromatograms obtained from the reaction mixture after 2.5 h catalysis by $Ag\text{-}Pd/ZrO_2$ under LSPR excitation (light irradiation) **(A)** and dark **(B)** conditions.

Table 1: Summary of the conversion and selectivity for the nitrobenzene reduction. Conversion and product selectivity for nitrobenzene reduction reaction under LSPR excitation and dark conditions. Peaks are not detected (ND) if their area is less than 10 000 counts. $Ag\text{-}Pd/ZrO_2$ and Ag/ZrO_2 were employed as catalysts and a blank reaction without any catalyst was also analyzed. Reaction conditions: catalyst (30 mg), solvent (IPA, 5 ml), base (KOH, 0.2 mmol/L) and reactant

(nitrobenzene, 0.15 mmol/L), under Ar atmosphere, 2.5 h at 70 °C.

Figure 6: Conversion percentage and selectivity under light illumination. (A) Nitrobenzene conversion under 425 nm light irradiation and in the dark for the reaction catalyzed by Ag-Pd/ZrO_2 (blue bar) and Ag/ZrO_2 (red bar). **(B)** Aniline and azobenzene selectivity under light irradiation for the reaction catalyzed by Ag-Pd/ZrO_2 (blue bars) and Ag/ZrO_2 (red bars).

DISCUSSION:

The findings described in this method demonstrate that the intrinsic catalytic activity of Pd (or other catalytic but not plasmonic metal) can be significantly enhanced by LSPR excitation *via* visible-light irradiation in bimetallic alloyed NPs[35]. In this case, Ag (or another plasmonic metal) is capable of harvesting energy from visible-light irradiation via LSPR excitation. The LSPR excitation leads to the formation of hot charge carriers (hot electrons and holes) and localized heating[5, 14–19]. While localized heating can contribute to enhanced reaction rates, the LSPR-excited charge carriers can participate in the vibrational or electronic activation of surface adsorbates[5, 14–19]. This allows for not only increased reaction rates but also changes in reaction selectivity due to selective activation of adsorbates or molecular orbitals at the metal-molecule interface, for example[20–25]. The method described herein effectively allows for the merging of plasmonic and catalytic properties in alloyed nanoparticle systems to extend the applicability of plasmonic catalysis to metals that are important in catalysis but do not support LSPR excitation in the visible range. Although the method described here focused on Ag and Pd as the plasmonic and catalytic metals, it can also be applied and adapted to other plasmonic catalytic combinations such as (Ag-Pt, Au-Pd, Au-Pt, etc.). Moreover, the plasmonic and catalytic properties of the bimetallic alloyed NPs can be further tuned by varying the relative molar ratios of the plasmonic and catalytic components. For instance, increasing the amount of Pd would make the nanoparticles more catalytic, while an increase in the Ag content leads to an increase in the optical properties. The synthesis method can also be adapted to achieve core-shell systems via the sequential deposition and reduction of precursors, for example[36]. It is noteworthy that there is also the possibility to extend the scope on the choice of plasmonic components to earth-abundant materials that can also be employed as supports. Examples include metal nitrides (TiN and ZrN) and some oxides (MoO_3) which support LSPR excitation in the visible and near-IR ranges[37–40].

In addition to the scope of the catalytic materials, the method presented in this paper can be applied to several types of liquid phase transformations that include other reductions, oxidations, and coupling reactions, for example[18]. Another advantage of this method is that the lamp's wavelength and number can be changed, which makes possible the study of the impact of the light's intensity and wavelength on the photocatalytic reaction. Wavelength-dependent photocatalytic reactions have been used to correlate the plasmonic properties of photocatalysts to their performance[5, 14–19]. It has been established increased plasmonic catalytic performances are observed when the light wavelength has a better matching to the LSPR extinction position[5, 14–19].

Finally, to be sure that the results are correct and representative, it is important to pay attention to some crucial steps of the protocol. When synthesizing the NPs, the amount of metal precursors

added in the reactor must be precisely known. Indeed, a small error on the Pd content, which is exceptionally low, can result in a dramatic change in the catalytic properties. After the synthesis, the drying temperature should not exceed 60 °C, as it would result in possible oxidation of the silver or aggregation of the NPs, once again interfering with the catalytic activity. The atmosphere of the photocatalytic reaction should also be controlled with great care. In our case, if the reactor is opened, the presence of an ambient atmosphere will put an end to the reaction. Thus, if these issues are well controlled, the method presented here can be used to study the plasmonic catalytic activity and selectivity of various plasmonic catalysts toward a wide range of chemical reactions. This can enable a better understanding of plasmonic catalysis and aid to the design of catalytic systems having target activities and selectivity for a reaction of interest under mild and environmentally friendly conditions.

ACKNOWLEDGMENTS:

This work was supported by the University of Helsinki and the Jane and Aatos Erkko Foundation. S.H. thanks Erasmus+ EU funds for the fellowship.

DISCLOSURES:

The authors have nothing to disclose.

REFERENCES:

1. Dunn, P.J., Hii, K.K. (MIMI), Krische, M.J., Williams, M.T. *Sustainable Catalysis: Challenges and Pratices for the Pharmaceutical and Fine Chemical Industries*. Wiley-Blackwell. (2013).
2. Tzouras, N. V., Stamatopoulos, I.K., Papastavrou, A.T., Liori, A.A., Vougioukalakis, G.C. Sustainable metal catalysis in C–H activation. *Coordination Chemistry Reviews*. **343**, 25–138, doi: 10.1016/j.ccr.2017.04.012 (2017).
3. Polshettiwar, V., Varma, R.S. Green chemistry by nano-catalysis. *Green Chemistry*. **12** (5), 743, doi: 10.1039/b921171c (2010).
4. Rodrigues, T.S., da Silva, A.G.M., Camargo, P.H.C. Nanocatalysis by noble metal nanoparticles: controlled synthesis for the optimization and understanding of activities. *Journal of Materials Chemistry A*. **7** (11), 5857–5874, doi: 10.1039/C9TA00074G (2019).
5. Linic, S., Christopher, P., Ingram, D.B. Plasmonic-metal nanostructures for efficient conversion of solar to chemical energy. *Nature Materials*. **10** (12), 911–921, doi: 10.1038/nmat3151 (2011).
6. Nam, J.M., Liz-Marzán, L., Halas, N. Chemical Nanoplasmonics: Emerging Interdisciplinary Research Field at Crossroads between Nanoscale Chemistry and Plasmonics. *Accounts of chemical research*. **52** (11), 2995–2996, doi: 10.1021/acs.accounts.9b00504 (2019).
7. Brongersma, M.L., Halas, N.J., Nordlander, P. Plasmon-induced hot carrier science and technology. *Nature Nanotechnology*. **10** (1), 25–34, doi: 10.1038/nnano.2014.311 (2015).
8. Smith, J.G., Faucheaux, J.A., Jain, P.K. Plasmon resonances for solar energy harvesting: A mechanistic outlook. *Nano Today*. **10** (1), 67–80, doi: 10.1016/j.nantod.2014.12.004 (2015).
9. Hartland, G. V. Optical studies of dynamics in noble metal nanostructures. *Chemical*

Reviews. **111** (6), 3858–3887, doi: 10.1021/cr1002547 (2011).
10. Kelly, K.L., Coronado, E., Zhao, L.L., Schatz, G.C. The optical properties of metal nanoparticles: The influence of size, shape, and dielectric environment. *Journal of Physical Chemistry B*. **107** (3), 668–677, doi: 10.1021/jp026731y (2003).
11. Hermoso, W., Alves, T. V., de Oliveira, C.C.S., Moriya, E.G., Ornellas, F.R., Camargo, P.H.C. Triangular metal nanoprisms of Ag, Au, and Cu: Modeling the influence of size, composition, and excitation wavelength on the optical properties. *Chemical Physics*. **423**, 142–150, doi: 10.1016/j.chemphys.2013.07.008 (2013).
12. Kumar, A., Reddy, K.L., Kumar, S., Kumar, A., Sharma, V., Krishnan, V. Rational Design and Development of Lanthanide-Doped NaYF4@CdS-Au-RGO as Quaternary Plasmonic Photocatalysts for Harnessing Visible-Near-Infrared Broadband Spectrum. *ACS Applied Materials and Interfaces*. **10** (18), 15565–15581, doi: 10.1021/acsami.7b17822 (2018).
13. Reddy, K.L., Kumar, S., Kumar, A., Krishnan, V. Wide spectrum photocatalytic activity in lanthanide-doped upconversion nanophosphors coated with porous TiO2 and Ag-Cu bimetallic nanoparticles. *Journal of Hazardous Materials*. **367** (August 2018), 694–705, doi: 10.1016/j.jhazmat.2019.01.004 (2019).
14. Ingram, D.B., Linic, S. Water splitting on composite plasmonic-metal/semiconductor photoelectrodes: Evidence for selective plasmon-induced formation of charge carriers near the semiconductor surface. *Journal of the American Chemical Society*. **133** (14), 5202–5205, doi: 10.1021/ja200086g (2011).
15. Linic, S., Aslam, U., Boerigter, C., Morabito, M. Photochemical transformations on plasmonic metal nanoparticles. *Nature Materials*. **14** (6), 567–576, doi: 10.1038/nmat4281 (2015).
16. Aslam, U., Rao, V.G., Chavez, S., Linic, S. Catalytic conversion of solar to chemical energy on plasmonic metal nanostructures. *Nat. Catal.* **1**, 656–665, doi: 10.1038/s41929-018-0138-x (2018).
17. Araujo, T.P., Quiroz, J., Barbosa, E.C.M., Camargo, P.H.C. Understanding plasmonic catalysis with controlled nanomaterials based on catalytic and plasmonic metals. *Current Opinion in Colloid and Interface Science*. **39**, 110–122, doi: 10.1016/j.cocis.2019.01.014 (2019).
18. Gellé, A., Jin, T., De La Garza, L., Price, G.D., Besteiro, L. V., Moores, A. Applications of plasmon-enhanced nanocatalysis to organic transformations. *Chemical Reviews*. 986–1041, doi: 10.1021/acs.chemrev.9b00187 (2020).
19. Shaik, F., Peer, I., Jain, P.K., Amirav, L. Plasmon-Enhanced Multicarrier Photocatalysis. *Nano Letters*. **18** (7), 4370–4376, doi: 10.1021/acs.nanolett.8b01392 (2018).
20. Quiroz, J. *et al.* Controlling Reaction Selectivity over Hybrid Plasmonic Nanocatalysts. *Nano Lett.* **18**, 7289–7297, doi: 10.1021/acs.nanolett.8b03499 (2018).
21. Peiris, E. *et al.* Plasmonic Switching of the Reaction Pathway: Visible-Light Irradiation Varies the Reactant Concentration at the Solid–Solution Interface of a Gold–Cobalt Catalyst. *Angewandte Chemie - International Edition*. **58** (35), 12032–12036, doi: 10.1002/anie.201904452 (2019).
22. Yu, S., Wilson, A.J., Heo, J., Jain, P.K. Plasmonic Control of Multi-Electron Transfer and C-C Coupling in Visible-Light-Driven CO2 Reduction on Au Nanoparticles. *Nano Letters*. **18** (4), 2189–2194, doi: 10.1021/acs.nanolett.7b05410 (2018).

23. Yu, S., Jain, P.K. Plasmonic photosynthesis of C 1 –C 3 hydrocarbons from carbon dioxide assisted by an ionic liquid. *Nature Communications*. **10**, 2022, doi: 10.1038/s41467-019-10084-5 (2019).
24. Zhang, X. *et al.* Product selectivity in plasmonic photocatalysis for carbon dioxide hydrogenation. *Nature Communications*. **8**, 1–9, doi: 10.1038/ncomms14542 (2017).
25. Cortés, E. Efficiency and Bond Selectivity in Plasmon-Induced Photochemistry. *Advanced Optical Materials*. **5** (15), 1700191, doi: 10.1002/adom.201700191 (2017).
26. de Freitas, I.C. *et al.* Design-controlled synthesis of IrO 2 sub-monolayers on Au nanoflowers: marrying plasmonic and electrocatalytic properties . *Nanoscale*. 23–27, doi: 10.1039/d0nr01875a (2020).
27. Zhang, C. *et al.* Al-Pd Nanodisk Heterodimers as Antenna-Reactor Photocatalysts. *Nano Letters*. **16** (10), 6677–6682, doi: 10.1021/acs.nanolett.6b03582 (2016).
28. Zhou, L. *et al.* Light-driven methane dry reforming with single atomic site antenna-reactor plasmonic photocatalysts. *Nature Energy*. **5**, 61–70, doi: 10.1038/s41560-019-0517-9 (2020).
29. Swearer, D.F. *et al.* Heterometallic antenna−reactor complexes for photocatalysis. *Proceedings of the National Academy of Sciences*. **113** (32), 8916–8920, doi: 10.1073/pnas.1609769113 (2016).
30. Peiris, S., Sarina, S., Han, C., Xiao, Q., Zhu, H.-Y. Silver and palladium alloy nanoparticle catalysts: reductive coupling of nitrobenzene through light irradiation. *Dalton Transactions*. **46** (32), 10665–10672 (2017).
31. Rahm, J.M. *et al.* A Library of Late Transition Metal Alloy Dielectric Functions for Nanophotonic Applications. *Advanced Functional Materials*. **2002122**, doi: 10.1002/adfm.202002122 (2020).
32. Zhang, C., Chen, B.Q., Li, Z.Y., Xia, Y., Chen, Y.G. Surface Plasmon Resonance in Bimetallic Core-Shell Nanoparticles. *Journal of Physical Chemistry C*. **119** (29), 16836–16845, doi: 10.1021/acs.jpcc.5b04232 (2015).
33. Liu, Z., Huang, Y., Xiao, Q., Zhu, H. Selective reduction of nitroaromatics to azoxy compounds on supported Ag-Cu alloy nanoparticles through visible light irradiation. *Green Chemistry*. **18** (3), 817–825, doi: 10.1039/x0xx00000x (201AD).
34. Chaiseeda, K., Nishimura, S., Ebitani, K. Gold nanoparticles supported on alumina as a catalyst for surface plasmon-enhanced selective reductions of nitrobenzene. *ACS Omega*. **2** (10), 7066–7070, doi: 10.1021/acsomega.7b01248 (2017).
35. Peiris, S. *et al.* Metal nanoparticle photocatalysts: emerging processes for green organic synthesis. *Catal. Sci. Technol.* **6** (2), 320–338, doi: 10.1039/C5CY02048D (2016).
36. García-García, I. *et al.* Silver-Based Plasmonic Catalysts for Carbon Dioxide Reduction. *ACS Sustainable Chemistry and Engineering*. **8** (4), 1879–1887, doi: 10.1021/acssuschemeng.9b06146 (2020).
37. Agrawal, A., Johns, R.W., Milliron, D.J. Control of Localized Surface Plasmon Resonances in Metal Oxide Nanocrystals. *Annual Review of Materials Research*. **47** (1), 1–31, doi: 10.1146/annurev-matsci-070616-124259 (2017).
38. Lounis, S.D., Runnerstrom, E.L., Llordés, A., Milliron, D.J. Defect chemistry and Plasmon physics of colloidal metal oxide Nanocrystals. *Journal of Physical Chemistry Letters*. **5** (9), 1564–1574, doi: 10.1021/jz500440e (2014).

39. Rej, S. *et al.* Determining Plasmonic Hot Electrons and Photothermal Effects during H2 Evolution with TiN–Pt Nanohybrids. *ACS Catalysis*. **10** (9), 5261–5271, doi: 10.1021/acscatal.0c00343 (2020).
40. Barragan, A.A. *et al.* Photochemistry of Plasmonic Titanium Nitride Nanocrystals. *The Journal of Physical Chemistry C*. **123** (35), 21796–21804, doi: 10.1021/acs.jpcc.9b06257 (2019).

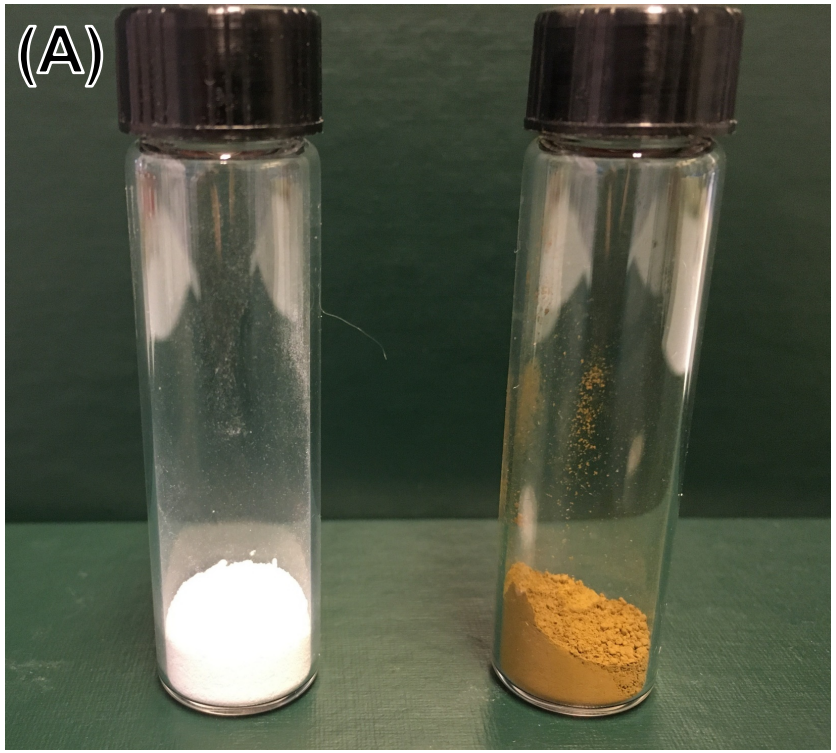
(A)
ZrO_2
Ag-Pd/ZrO_2

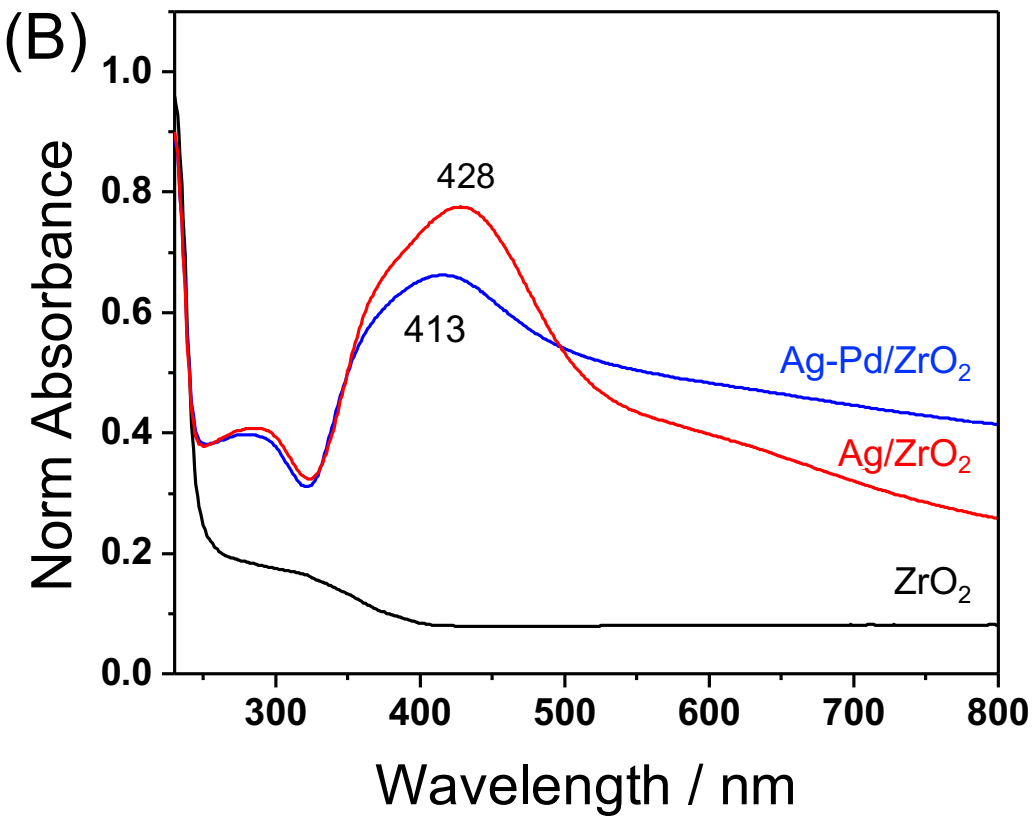
(B)
Norm Absorbance
1.0
0.8
0.6
0.4
0.2
0.0
300
400
500
600
700
800
Wavelength / nm
428
413
Ag-Pd/ZrO_2
Ag/ZrO_2
ZrO_2

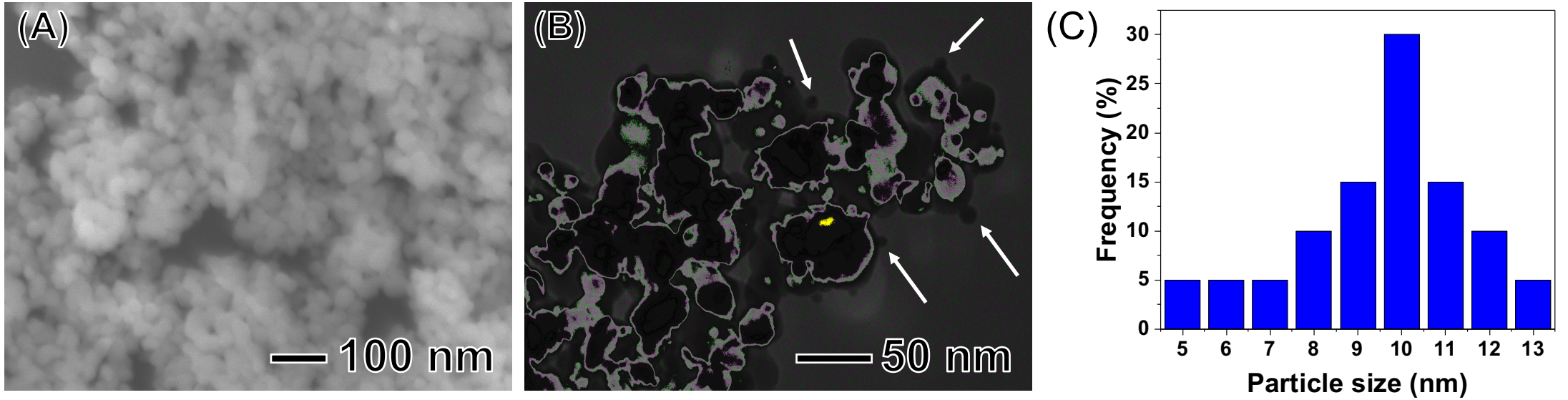
(A)
100 nm
(B)
50 nm
(C)
Frequency (%)
0
5
10
15
20
25
30
5
6
7
8
9
10
11
12
13
Particle size (nm)

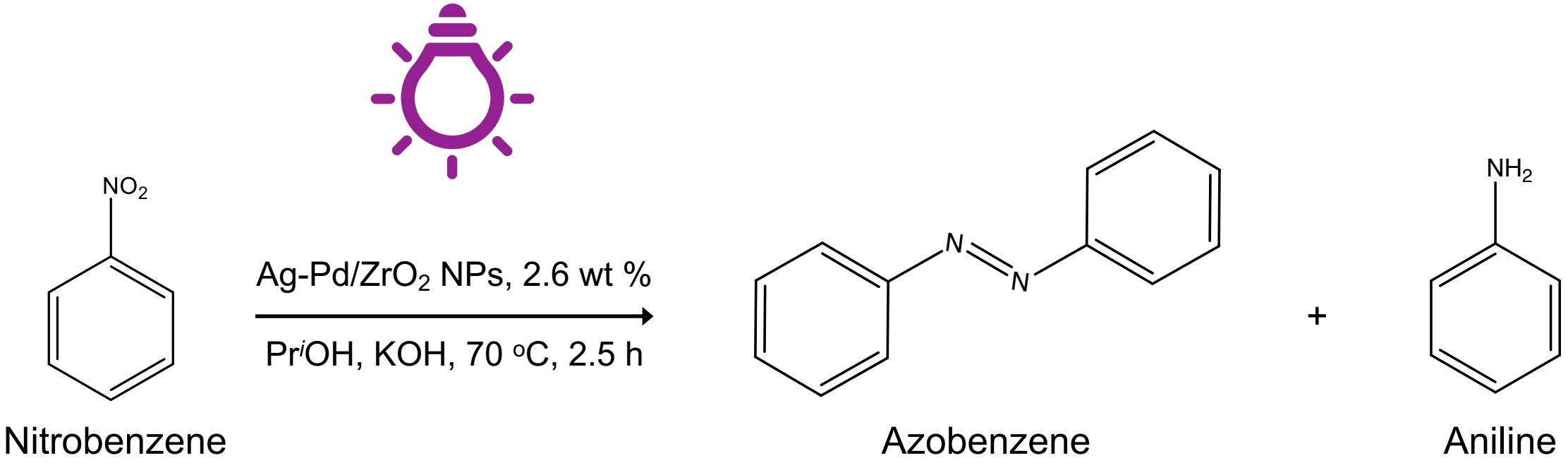
NO2
Ag-Pd/ZrO2 NPs, 2.6 wt %
PriOH, KOH, 70 oC, 2.5 h
N
N
+
NH2
Nitrobenzene
Azobenzene
Aniline

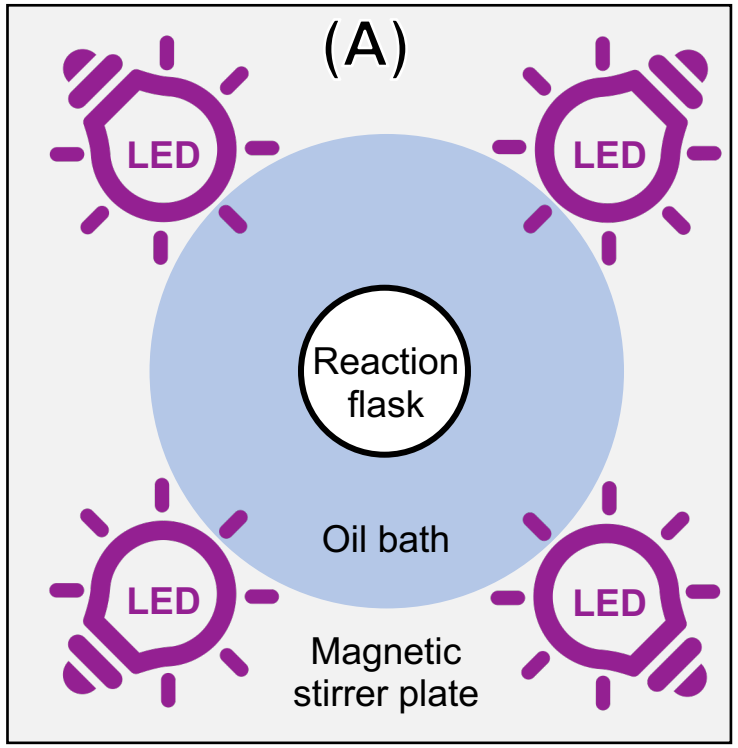
(A)
LED
LED
Reaction flask
Oil bath
LED
LED
Magnetic stirrer plate

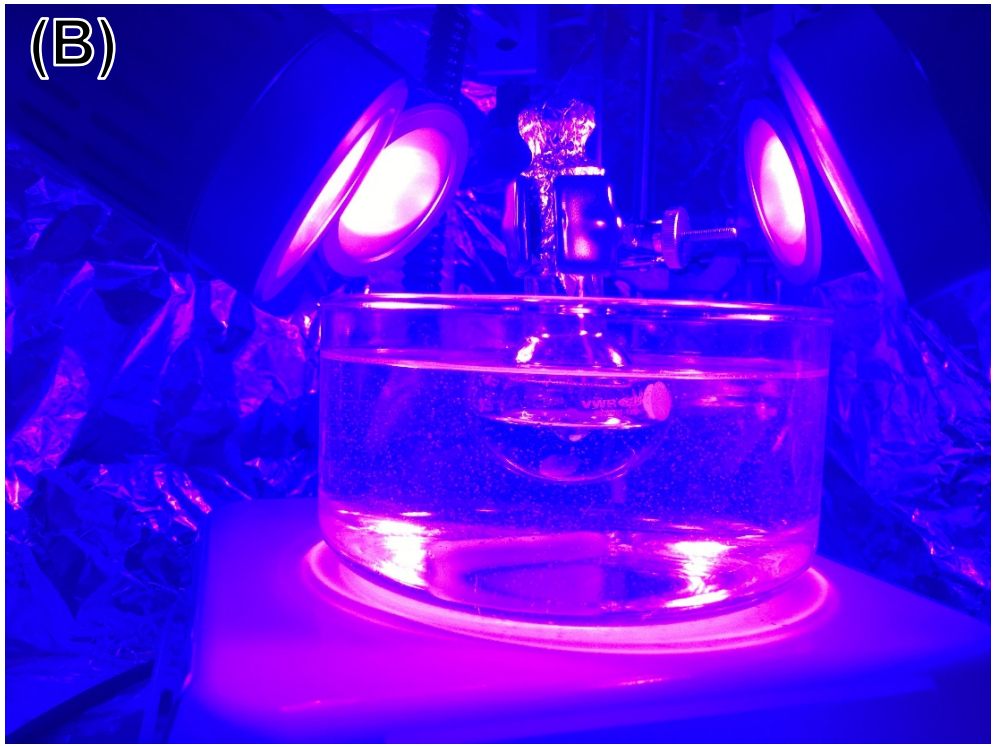
(B)

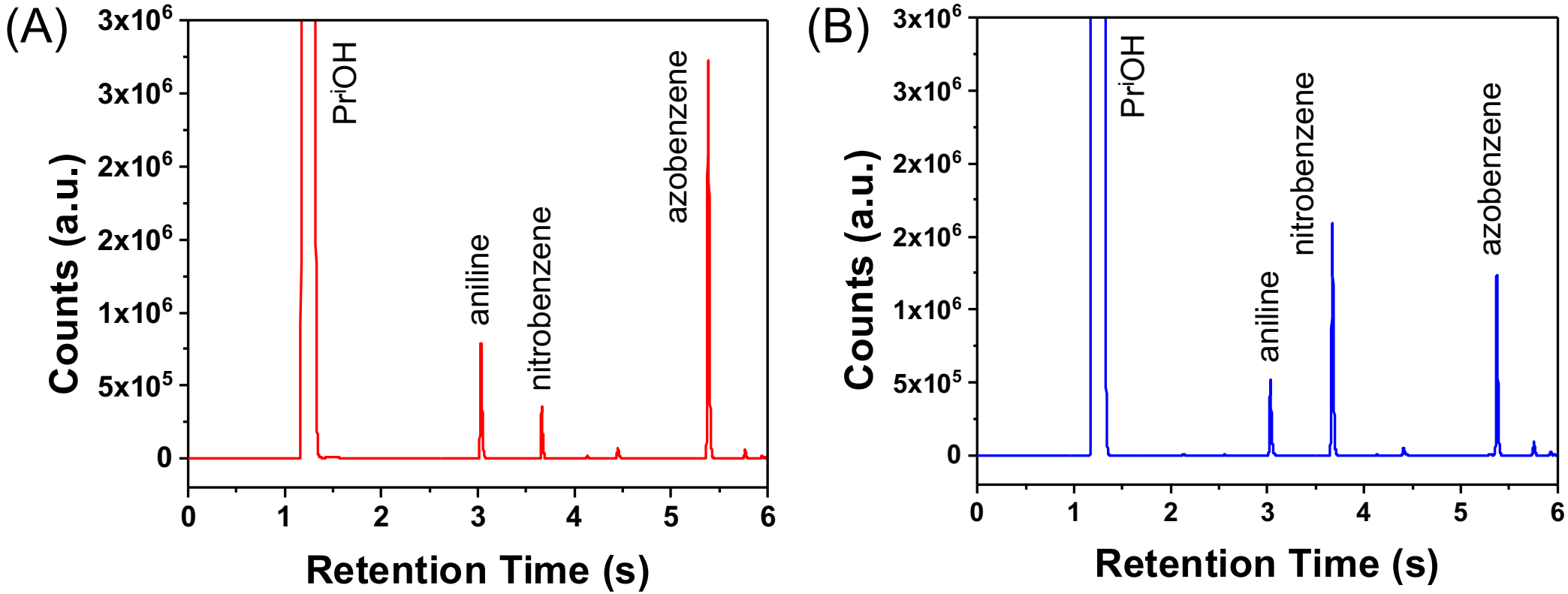
(A)
Counts (a.u.)
3x10^6
3x10^6
2x10^6
2x10^6
1x10^6
5x10^5
0
PrⁱOH
aniline
nitrobenzene
azobenzene
0
1
2
3
4
5
6
Retention Time (s)
(B)
Counts (a.u.)
3x10^6
3x10^6
2x10^6
2x10^6
1x10^6
5x10^5
0
PrⁱOH
aniline
nitrobenzene
azobenzene
0
1
2
3
4
5
6
Retention Time (s)

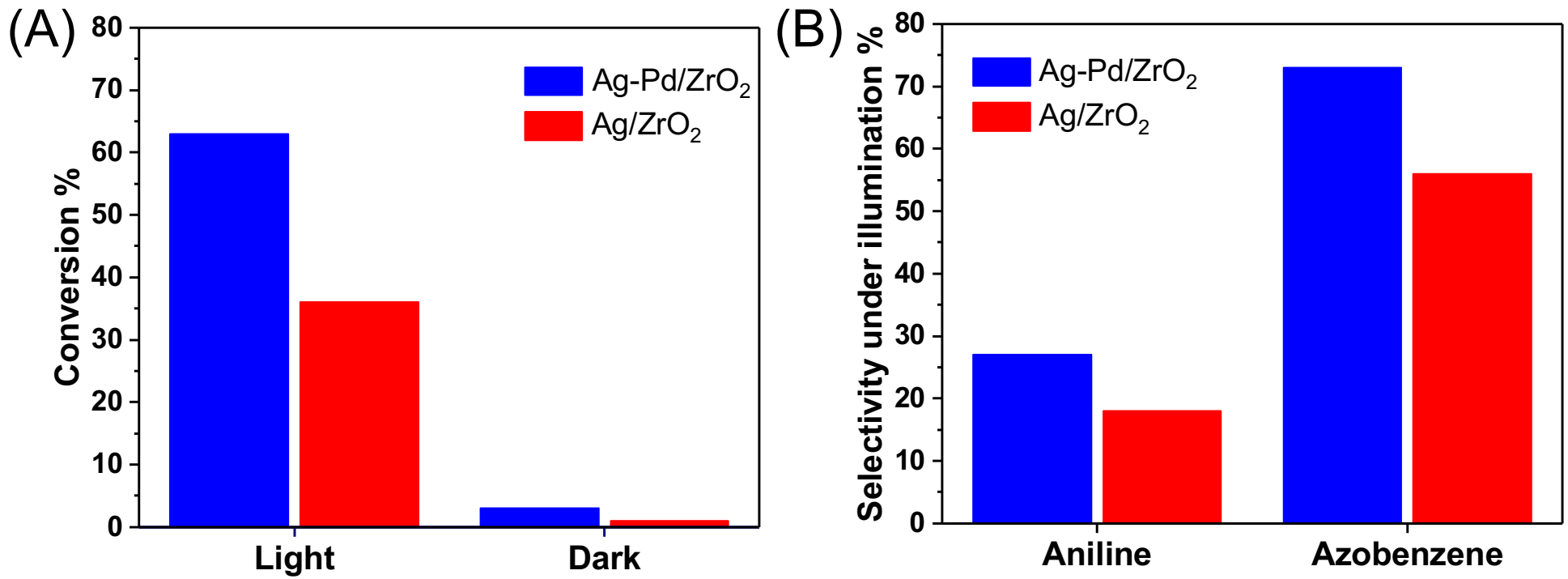
(A)
Conversion %
80
70
60
50
40
30
20
10
0
Ag-Pd/ZrO2
Ag/ZrO2
Light
Dark
(B)
Selectivity under illumination %
80
70
60
50
40
30
20
10
0
Ag-Pd/ZrO2
Ag/ZrO2
Aniline
Azobenzene